Dopant Incorporation in Colloidal Quantum Dots: A Case Study on Co^{2+} Doped ZnO

Petra Lommens,*,† Frank Loncke,‡ Philippe F. Smet,‡ Freddy Callens,‡ Dirk Poelman,‡ Henk Vrielinck,‡ and Zeger Hens†

Physics and Chemistry of Nanostructures, Ghent University, B-9000 Ghent, Belgium, and Department of Solid State Sciences, Ghent University, B-9000 Ghent, Belgium

Received June 18, 2007. Revised Manuscript Received August 24, 2007

We demonstrate that three different types of Co^{2+} ions are present in Co^{2+} doped colloidal ZnO (Co:ZnO) quantum dots. First, absorbance and luminescence spectroscopy confirm that part of the Co^{2+} ions replace Zn^{2+} ions in the Co:ZnO core. Furthermore, an amine surface treatment reveals that an important fraction of the Co^{2+} ions only adsorbs at the nanocrystal surface. In addition, the electron paramagnetic resonance (EPR) spectrum of Co:ZnO quantum dot powders contains contributions of two types of Co^{2+} ions. On the basis of simulations of the EPR spectra, we conclude that a first contribution is related to substitutional Co^{2+}, while the second is due to Co^{2+} ions in an octahedral coordination. Because the EPR spectrum does not change after amine surface treatment, we conclude that these so-called type III Co^{2+} ions are present in the core of the Co:ZnO quantum dots, and we suggest that they might correspond with interstitial Co^{2+} ions. By growing a ZnO shell around the Co:ZnO core, we demonstrate that adsorbed Co^{2+} ions can be incorporated in the nanocrystals both as substitutional and type III Co^{2+} ions. Magnetic measurements as a function of magnetic field down to 4.5 K only show a paramagnetic behavior with all three types of Co^{2+} contributing with a spin $S = {}^3/_2$ to the total magnetization.

1. Introduction

The addition of well-chosen impurities or doping is probably the most widely used technique to alter the electric and optical properties of a bulk semiconductor. Following the development of colloidal routes for semiconductor nanocrystal synthesis, doping has been explored extensively over the last 10 years as a technique to modify the properties of colloidal semiconductor nanocrystals or quantum dots. For instance, II−VI semiconductors like ZnS,[1] CdSe,[2] and ZnO[3] have been doped with Mn or rare earth elements to change their photoluminescence properties, doping of CdSe quantum dots with K can increase their conductivity,[4] and transition metal ions have been incorporated into ZnO nanocrystals leading to high-temperature ferromagnetic nanocrystal aggregates.[5]

Many of these studies have indicated that dopant incorporation in the core of colloidal nanocrystals is problematic.[4,6,7] Colloidal nanocrystals contain ∼10 000 atoms at the most. This means that dopant densities will always be relatively high, which may render doping impossible if the dopant solubility is low. However, even for highly soluble dopants, the incorporation of a significant amount of dopant atoms during synthesis is not straightforward. Poor adsorption of dopants at the nanocrystal surface or strong complexation of dopant precursors in solution may prevent the formation of doped nanocrystals.[6] As a result, many colloidal synthesis procedures lead to nanocrystals where dopants are only adsorbed at the nanocrystal surface, if not washed away during purification.

Transition metal doping of ZnO has become an active field of research ever since it was predicted to lead to room-temperature ferromagnetism.[8,9] Apart from leading to applications,[10,11] ZnO quantum dots offer several advantages over bulk ZnO for studying the properties of transition metal dopants. Quantum confinement effects enable one to monitor delocalization of electronic states and give rise to superior optical properties. Furthermore, with nanocrystalline powders, considerable particle growth can be achieved by annealing at temperatures as low as 300 °C. This means that a decrease of the surface-to-volume ratio can be realized without risking phase segregation or the formation of new

* To whom correspondence should be addressed. E-mail: Petra.Lommens@UGent.be.
† Physics and Chemistry of Nanostructures, Ghent University.
‡ Department of Solid State Sciences, Ghent University.

(1) Borse, P. H.; Srinivas, D.; Shinde, R. F.; Date, S. K.; Vogel, W.; Kulkarni, S. K. *Phys. Rev. B* **1999**, *60*, 8659.
(2) Mikulec, F. V.; Kuno, M.; Bennati, M.; Hall, D. A.; Griffin, R. G.; Bawendi, M. G. *J. Am. Chem. Soc.* **2000**, *122*, 2532.
(3) Pereira, A. S.; Peres, M.; Soares, M. J.; Alves, E.; Neves, A.; Monteiro, T.; Trindade, T. *Nanotechnology* **2006**, *17*, 834.
(4) Yu, D.; Wang, C. J.; Guyot-Sionnest, P. *Science* **2003**, *300*, 1277.
(5) Schwartz, D. A.; Norberg, N. S.; Nguyen, Q. P.; Parker, J. M.; Gamelin, D. R. *J. Am. Chem. Soc.* **2003**, *125*, 13205.
(6) Erwin, S. C.; Zu, L. J.; Haftel, M. I.; Efros, A. L.; Kennedy, T. A.; Norris, D. J. **2005**, *436*, 91.
(7) Dalpian, G. M.; Chelikowsky, J. R. *Phys. Rev. Lett.* **2006**, *96*, 226802.
(8) Dietl, T.; Ohno, H.; Matsukura, F.; Cibert, J.; Ferrand, D. *Science* **2000**, *287*, 1019.
(9) Sato, K.; Katayama-Yoshida, H. *Semicond. Sci. Technol.* **2002**, *17*, 367.
(10) Liu, W. K.; Salley, G. M.; Gamelin, D. R. *J. Phys. Chem. B* **2005**, *109*, 14486.
(11) Wolf, S. A.; Awschalom, D. D.; Buhrman, R. A.; Daughton, J. M.; von Molnar, S.; Roukes, M. L.; Chtchelkanova, A. Y.; Treger, D. M. *Science* **2001**, *294*, 1488.

10.1021/cm071623f CCC: $37.00
Published on Web 10/12/2007

compounds, which could have impact on, e.g., magnetic properties. Nevertheless, the use of doped colloidal quantum dots also raises important questions, especially regarding the incorporation of the dopants in the nanocrystal lattice.

Here, we exemplify these complications of dopant incorporation in colloidal nanocrystals by a case study on Co^{2+} doped ZnO (Co:ZnO) quantum dots. This is a well-chosen model system since the Co^{2+} ion can be investigated with a number of complementary spectroscopic techniques. Using UV−vis spectrophotometry, spectrofluorometry, and electron paramagnetic resonance (EPR) spectroscopy, we demonstrate that three different types of Co^{2+} ions should be distinguished in Co:ZnO quantum dots. First, substitutional Co^{2+} ions can be identified by UV−vis and luminescence spectroscopy. Second, the presence of surface-adsorbed Co^{2+} ions is demonstrated by an octylamine surface treatment and by the growth of and additional ZnO shell around the Co:ZnO particles. Finally, the existence of a third type of Co^{2+} ions in Co:ZnO quantum dots is inferred from their EPR spectrum. This contains prominent features that cannot be interpreted using only substitutional and surface-adsorbed Co^{2+} ions. As these features can be related to octahedrally coordinated Co^{2+}, we tentatively identify these so-called type III Co^{2+} ions with Co^{2+} interstitials. On the basis of absorption and EPR measurements, we show that surface-adsorbed Co^{2+} ions are incorporated in the nanocrystal core both as substitutional and as type III interstitial ions. Magnetic measurements indicate that all Co^{2+} ions contribute with $S = {}^3/_2$ to the paramagnetic magnetization of the Co:ZnO powders.

2. Experimental Section

2.1. Nanocrystal Synthesis. We prepared Co^{2+} doped ZnO nanocrystals according to the wet chemical route described by Schwartz et al.[5] The precursor salts ($ZnAc_2$ and $CoAc_2 \cdot 4H_2O$) were dissolved in 15 mL of dimethylsulfoxide (DMSO), keeping the total metal ion concentration at 0.1 mol/L. A sample of 2.5 mmol of $(CH_3)_4NOH \cdot 5H_2O$ (TMAH), dissolved in 5 mL of dry ethanol, was added dropwise to the metal salt solution under vigorous stirring at room temperature. The resulting nanocrystals could be precipitated by adding 40 mL of ethylacetate. After removal of the supernatant, the nanocrystals were resuspended in 20 mL of dry ethanol. The nanocrystals could be precipitated again by adding 40 mL of heptane, to be resuspended once more in 20 mL of dry ethanol. The powder aggregates used for EPR, X-ray diffraction (XRD), and inductively coupled plasma mass spectrometry (ICP−MS) measurements were obtained by vacuum drying of nanocrystals precipitated from a doubly washed suspension in ethanol.

2.2. Amine Treatment. Octylamine (3 mL) was added to an equal volume of Co:ZnO nanocrystals in a 1:1 mixture of EtOH/DMSO. The resulting turbid mixture was heated for 2 h at 45 °C. Afterward, the nanocrystals were removed from the supernatant by centrifugation. These nanocrystals could be resuspended in $CHCl_3$, indicating the presence of a long-chain amine ligand shell. In order to obtain powder aggregates, the octylamine capped nanocrystals were precipitated with ethanol and dried under vacuum.

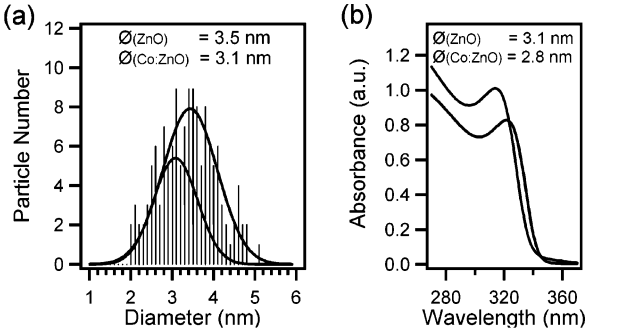

Figure 1. (a) Particle-size distributions obtained from TEM measurements on a ZnO (—) and a Co:ZnO (—) suspension. A Gaussian fit to both histograms was included as a guide to the eye. (b) Band gap absorbance spectra for the same ZnO and 2% Co:ZnO suspensions. In both (a) and (b), the particle sizes obtained from the respective measurements are shown.

2.3. Core/Shell Synthesis. After washing a 2% Co:ZnO suspension, we repeatedly added extra precursor salts in order to grow a shell of pure ZnO around the Co:ZnO cores. For instance, to a washed 10 mL Co:ZnO suspension (Ø = 2.8 nm), 3 mL of a 0.075 M $Zn(Ac)_2$ solution in DMSO was added first, followed by 1 mL of a 0.375 M TMAH solution in EtOH. After adding the extra salts, the mixture was heated to 50 °C for 5 min and cooled down to room temperature. As checked by absorption spectroscopy and transmission electron microscopy (TEM), repeating this procedure 10 times led to a 1 nm increase of the mean nanocrystal diameter, while the nanocrystal diameter only slightly changed by 0.2 nm when the heating cycles were performed without the additional precursor salts added.

2.4. Characterization. The crystal structure of the nanocrystals was investigated using a Siemens D5000 X-ray diffractometer in $\theta/2\theta$ mode, using Cu Kα radiation. Dopant concentrations after synthesis were determined analytically using ICP−MS (Perkin-Elmer SCIEX Elan 5000), for which powder aggregates were dissolved in 1.3% HNO_3. TEM and high-resolution TEM (HR-TEM) measurements were obtained on a Jeol 2200FS transmission electron microscope. Absorption spectra were collected with a Cary 500 UV−vis-NIR spectrophotometer (Varian) using quartz cuvettes with an optical path length of 1 cm. By TEM measurements on different Co:ZnO and ZnO samples, we verified that particle sizes of 2% Co:ZnO can still be inferred from the energetic position of the band-edge absorption using the relation proposed by Meulenkamp for pure ZnO.[12] As an example, Figure 1 shows the particle-size distribution and mean diameter obtained by TEM analysis of ZnO and 2% Co:ZnO particles, together with the corresponding absorption spectrum. In both cases, a fair agreement between the average TEM diameter and the diameter inferred from the absorption spectrum is obtained. For measuring steady-state photoluminescence (PL) spectra, a FS920 luminescence spectrometer from Edinburgh Instruments was used. Q-band ($\nu = 34$ GHz) EPR measurements on nanocrystal powder aggregates were performed using a Bruker Elexsys E500, equipped with an

(12) Meulenkamp, E. A. *J. Phys. Chem. B* **1998**, *102*, 5566.

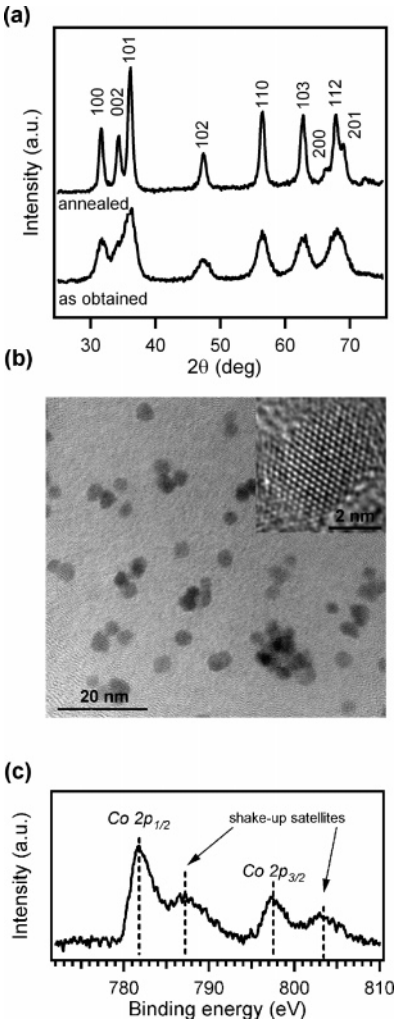

Figure 2. (a) Powder θ-2θ XRD spectra for 2% Co:ZnO nanocrystalline powders as obtained after synthesis and after heating for 2 h at 300 °C under air. (b) TEM image of 2% Co:ZnO quantum dots (d = 3.7 nm from UV−vis); inset = high-resolution image. (c) Co 2p XPS spectrum of a dropcast layer of 2% Co:ZnO nanocrystals.

Oxford CF935 cryostat. The modulation amplitude was set at 2 G. EPR spectra have been analyzed using the EasySpin program package.[13] The magnetic properties of the powders were measured using a SQUID magnetometer (MPMS-Quantum Design).

3. Results

3.1. General Characterization. XRD measurements have been performed on as-obtained powder aggregates of ZnO nanocrystals nominally doped with 2% Co^{2+} ions and on powders that were annealed at 300 °C for 2 h. As can be seen from Figure 2a, both patterns are indicative of the hexagonal ZnO wurtzite crystal structure and no additional reflections due to related phases such as CoO, Co_3O_4, or Zn-$(OH)_2$ are present.[12,14] As confirmed by the narrowing of the XRD reflections, heat treatment for 2 h at 300 °C under aerobic conditions leads to particle growth. In Figure 2b, a TEM picture obtained with 2% Co:ZnO quantum dots (QDs) having an average diameter of 3.7 nm is shown. The high-resolution TEM inset confirms the crystallinity of the nanocrystals. X-ray photoelectron spectroscopy (XPS) measurements have been used to investigate the oxidation state of the cobalt ions (Figure 2b). The Co 2p XPS spectrum shows four peaks, a doublet and its corresponding shakeup satellites, at slightly higher energies. Binding energies of 781.9 and 797.6 eV have been found for Co $2p_{3/2}$ and $2p_{1/2}$, respectively. The energy difference of 15.7 eV between the two cobalt binding energies agrees with literature data on Co:ZnO and CoO.[15,16] Dopant concentrations after synthesis were determined analytically using ICP−MS. In a three-times-washed Co:ZnO sample, an average molar ratio of x_{Co} = 0.0204 was found for the Co^{2+} ions. Because three washing steps do not reduce the cobalt concentration below the nominal concentration, either all the Co^{2+} ions introduced during synthesis are incorporated in the ZnO nanocrystal or surface-adsorbed Co^{2+} ions cannot be removed by precipitating and resuspending the nanocrystals.

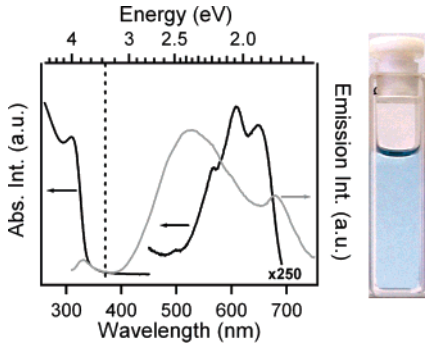

Figure 3. (—) Optical absorption spectrum of a 2% Co:ZnO nanocrystal (Ø = 2.7 nm) suspension in ethanol with the band-gap absorption on the left and the Co^{2+} ligand-field transitions on the right. The dashed line indicates the energetic position of the bulk band gap for ZnO. (—) Photoluminescence spectrum of the same suspension excited at λ = 280 nm. Inset = photograph of the Co:ZnO suspension.

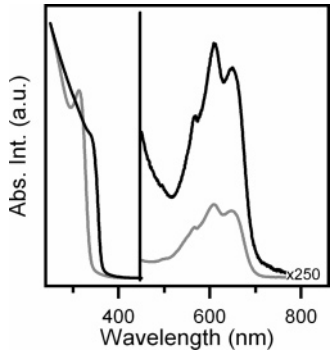

Figure 4. Optical absorption spectrum of a washed 2% Co:ZnO nanocrystal (Ø = 2.7 nm) suspension (—) and the same suspension after shell growth (Ø = 3.9 nm) (—). The band-edge absorption spectra were normalized at 250 nm. The ligand-field spectra have been correct for the dilution of the sample due to the shell-growth procedure.

3.2. Optical Characterization. The synthesis described in the Experimental Section results in a clear blue suspension containing 2% Co:ZnO quantum dots (Figure 3). Absorption spectra show the confined band gap absorption, indicative of a particle diameter of 2.7 nm in this case. The Co^{2+} ligand field absorption results in a structured band in the visible with maxima at 567, 611, and 652 nm, representing the $^4A_2$-

(13) Stoll, S.; Schweiger, A. *J. Magn. Reson.* **2006**, *178*, 42.
(14) Deka, S.; Joy, P. A. *Appl. Phys. Lett.* **2006**, *89*, 032508.
(15) Chuang, T. J.; Brundle, C. R.; Rice, D. W. *Surf. Sci.* **1976**, *59*, 413.
(16) Deka, S.; Joy, P. A. *Solid State Commun.* **2005**, *134*, 665.

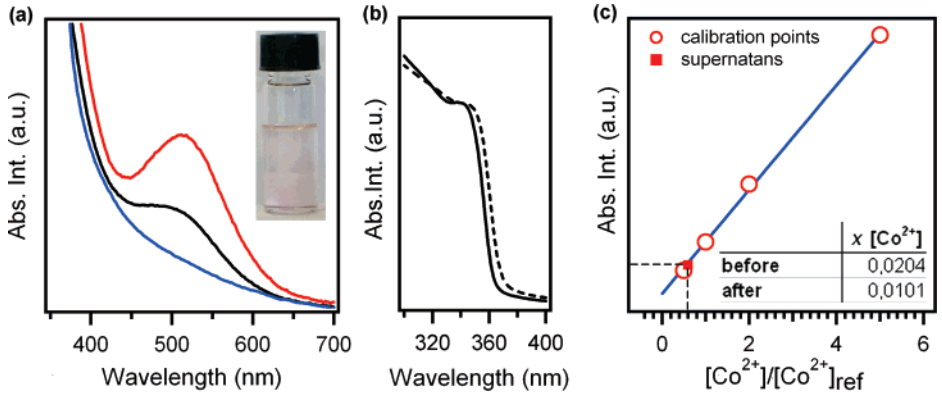

Figure 5. (a) Absorption spectra obtained for (—) the pink supernatant obtained after OA treatment of a suspension containing 2% Co:ZnO nanocrystals, (blue line) a 1:1:1 DMSO/EtOH/OA mixture, and (red line) a solution of $Co(Ac)_2$ (0.002M) in 1:1:1 DMSO/EtOH/OA; inset = photograph of the supernatant. (b) Band-edge absorption for the nanocrystals before (full) and after (dashed) amine treatment. (c) Calibration curve based on the absorption intensity of $Co(Ac)_2$ dissolved in a 1:1:1 DMSO/EtOH/OA mixture; inset = results obtained from ICP−MS analysis of a Co:ZnO sample before and after treatment with octylamine.

(F) → $^2A_1$(G), $^4T_1$(P), and $^2T_1$(G) transitions, typical for tetrahedrally coordinated Co^{2+} ions substituting for Zn^{2+} in the hexagonal ZnO wurtzite structure.[17]

A luminescence spectrum obtained from the same suspension excited at 280 nm is also shown in Figure 3. Three emission bands can be seen, at 330, 530, and 680 nm. The first band is due to exciton recombination; the defect emission at about 530 nm has been attributed to the recombination of an electron in the conduction band with a hole trapped in a defect level, probably an oxygen vacancy.[18] Finally, the emission at 680 nm is due to transitions between localized Co^{2+} *d*-levels, $^4T_1$(P), $^2T_1$(G), ^2E(G) → $^4A_2$(F).[19−21] The total luminescence intensity of these suspensions is very low; only 5% of the native ZnO defect luminescence remains after doping with 2% Co.

Figure 4 shows Co:ZnO absorption spectra before and after shell growth, corrected for dilution after shell growth. Two features of these spectra are of importance. First, the absorption onset shows a redshift from 330 to 360 nm, reflecting the increase of the nanocrystal diameter from 2.8 to 3.8 nm. Second, the intensity of the absorption related to substitutional Co^{2+} almost triples, indicating that shell growth strongly enhances the number of substitutional Co^{2+} ions in the nanocrystals.

3.3. Amine Surface Treatment. Adding octylamine (OA) to a washed suspension of Co:ZnO quantum dots leads to nanocrystal aggregation (see Experimental Section). A blue precipitate, which can be resuspended in $CHCl_3$, and a pink supernatant (inset Figure 5a) are formed. The supernatant shows the same Co^{2+}-related absorption features as that of $Co(Ac)_2$ dissolved in a 1:1:1 EtOH/DMSO/OA mixture, indicating that it contains OA-complexed Co^{2+} ions (Figure 5a). The band-edge absorption of the resulting OA-capped quantum dots in $CHCl_3$ does not show a blueshift. With Co:ZnO/ZnO core/shell particles, no Co^{2+}-related features appeared in the absorption spectrum of the supernatant after amine treatment.

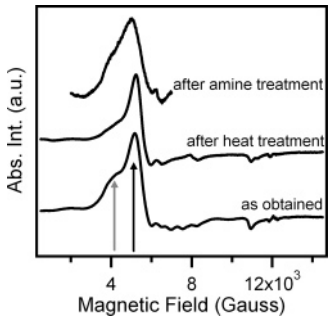

Figure 6. Q-band EPR spectra measured at 20 K and 34 GHz on 2% Co:ZnO nanocrystal aggregates as obtained after synthesis, after treatment with dodecylamine, and after heat treatment for 2 h at 300 °C. The arrows indicate the high-field and low-field components.

Figure 5c shows the Co^{2+} ligand field absorption intensity for five solutions containing different amounts of $Co(Ac)_2$ in a 1:1:1 mixture of EtOH/DMSO/OA. The calibration points were obtained by integrating the absorption spectra between 390 and 750 nm after removing an exponential background. The reference concentration $[Co^{2+}]_{ref}$ corresponds to the amount of Co^{2+} used during synthesis of a 2% Co:ZnO sample. Combining the absorbance of the supernatant with this calibration curve, we calculate that 50−60% of the Co^{2+} ions initially entering synthesis are retrieved in the supernatant after amine treatment. These results were confirmed by ICP−MS measurements on nanocrystals powders, which show a reduction of the Co content from $x_{Co} = 0.0204$ after washing but before amine treatment to $x_{Co} = 0.0101$ after amine treatment (inset of Figure 5c).

3.4. EPR Spectroscopy. Figure 6 shows a Q-band EPR spectrum measured at 20 K on an as-obtained 2% Co:ZnO nanocrystal powder. It shows a powder pattern typical of centers with $g_\perp^{eff} > g_\parallel^{eff}$, resulting in first-derivative spectra characterized by intense and broad $g_\perp$ ($g_x = g_y$) features with mainly positive signal intensity and weaker, more narrow $g_\parallel$ (g_z) features with negative signal intensity. The resonance at $g = 1.96$ (12 400 G), often encountered in ZnO samples and attributed to shallow donors, has not been detected. This might be due to broadening because of fast spin−spin

(17) Weakliem, H. A. *J. Chem. Phys.* **1962**, *36*, 2117.
(18) van Dijken, A.; Meulenkamp, E. A.; Vanmaekelbergh, D.; Meijerink, A. *J. Phys. Chem. B* **2000**, *104*, 1715.
(19) Lommens, P.; Smet, P. F.; Donega, C. D.; Meijerink, A.; Piraux, L.; Michotte, S.; Matefi-Tempfli, S.; Poelman, D.; Hens, Z. *J. Lumin.* **2006**, *118*, 245.
(20) Koidl, P. *Phys. Rev. B* **1977**, *15*, 2493.
(21) Schulz, H. J.; Thiede, M. *Phys. Rev. B* **1987**, *35*, 18.

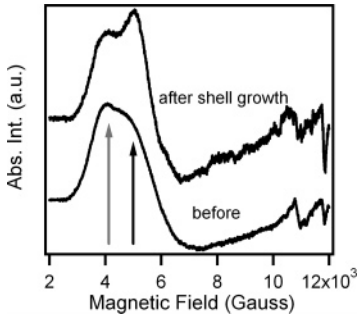

Figure 7. Q-band EPR spectra measured at 20 K and 34 GHz on 2% Co:ZnO nanocrystal aggregates as obtained after synthesis and after shell growth.

relaxation of the shallow donor electrons in the presence of many unpaired Co *d*-electrons.

For all measurements in Q-band and a control measurement in X-band, the positive $g_\perp$ ($g_x = g_y$) feature appearing between 3 500 and 6 000 G appears as a double peak or a peak with a shoulder at lower fields (as indicated with black and gray arrows in Figure 6). We extensively investigated whether different postsynthesis sample treatments affected the appearance of this part of the EPR spectrum. First, amine surface treatment, which removes ~50% of all Co^{2+} ions present, does not change the EPR intensity ratio of the two components. Second, heating the nanocrystals in air for 2 h at 300 °C leads to an increase in the main peak-to-shoulder intensity ratio and improves the resolution of the $g_{||}$ features (Figure 6). Finally, Figure 7 demonstrates that shell growth leads to a moderate increase of the high-field component relative to the low-field component after shell growth.

3.5. Magnetic Measurements. Figure 8a shows the magnetization per Co^{2+} ion as a function of the applied magnetic field for an as-obtained 2% Co:ZnO nanocrystalline powder. Both at room temperature and at 4.5 K, the magnetization vs magnetic field curve shows a typical paramagnetic behavior, without any sign of a ferromagnetic hysteresis loop. At high field strengths, the magnetization levels off because of the starting paramagnetic alignment of the magnetic moments. Literature reports almost complete alignment at field strengths above 6 T for 5% Co:ZnO single crystals at 2 K.[22] From the slope of the magnetization at low-field strength, we calculate an effective magnetic moment of 4.21 μ_B/Co^{2+} ion. This value is in line with literature data on polycrystalline[23] and single-crystal[22] Co:ZnO that show anisotropic magnetization behavior and agree reasonably well with the spin-only value of 3.87 μ_B/Co^{2+}.[24] A measurement of the magnetization as a function of temperature between 5 and 150 K (Figure 8b) could be fitted with a Curie−Weiss law ($1/\chi = (T - \Theta)/C$). A Curie−Weiss temperature Θ of 0.2 K and an effective magnetic moment of $\mu_{eff} = 3.91\ \mu_B/Co^{2+}$ was found. We conclude that all Co^{2+} ions contribute to the magnetic susceptibility with an effective magnetic moment of $S = {}^3/_2$.

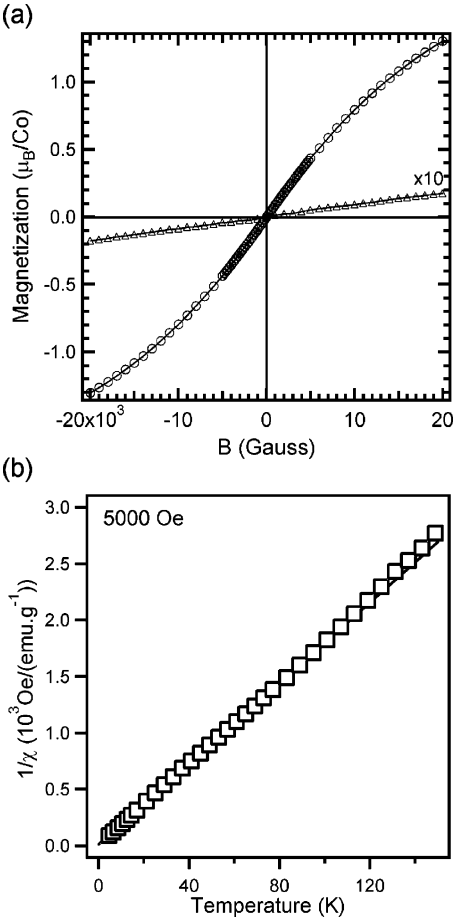

Figure 8. (a) Magnetic moment per Co^{2+} ion as a function of applied magnetic field at 4.5 K (○) and at 300 K (△) for a powder sample containing 2% Co ions. The magnetic moment per Co^{2+} ion was calculated based on ICP−MS measurements. (b) Inverse susceptibility of the same sample as a function of temperature measured at 5 000 Oe.

4. Discussion

4.1. Substitutional Co^{2+}. The optical absorption and PL measurements present clear evidence for the presence of tetrahedrally coordinated Co^{2+} ions replacing Zn^{2+} inside the ZnO quantum dots. Substitutional Co^{2+} gives a structured band in the visible absorption spectrum with maxima at 567, 611, and 652 nm and an emission at about 680 nm.

The EPR spectrum of substitutional Co^{2+} in ZnO is described by a spin Hamiltonian of the following kind:

$$\hat{H}_s = \mu_B(g_{||}B_z\hat{S}_z + g_\perp(B_x\hat{S}_x + B_y\hat{S}_y)) + \frac{D}{3}(\hat{S}_z{}^2 - \hat{S}^2) \quad (1)$$

This Hamiltonian complies with the fact that an oxygen ligand field of intermediate strength splits the ^4F ground state term of Co^{2+} ($3d^7$ $S = {}^3/_2$) ions into an orbital singlet ($^4A_2$) and two orbital triplets ($^4T_1$, $^4T_2$). In a tetrahedral coordination, like for substitutionally doped Co^{2+} ions in ZnO, the singlet lies lowest and the effective spin of the paramagnetic center corresponds to the electron spin, $S = {}^3/_2$. Because of the axial distortion of the crystal field in the hexagonal ZnO crystal, the Hamiltonian is completed with a zero-field

(22) Li, W.; Kang, Q. Q.; Lin, Z.; Chu, W. S.; Chen, D. L.; Wu, Z. Y.; Yan, Y.; Chen, D. G.; Huang, F. *Appl. Phys. Lett.* **2006**, *89*, 112507.
(23) Lawes, G.; Risbud, A. S.; Ramirez, A. P.; Seshadri, R. *Phys. Rev. B* **2005**, *71*, 045201.
(24) Jiles, D. *Introduction to Magnetism and Magnetic Materials*; Chapman & Hall: London, 1998.

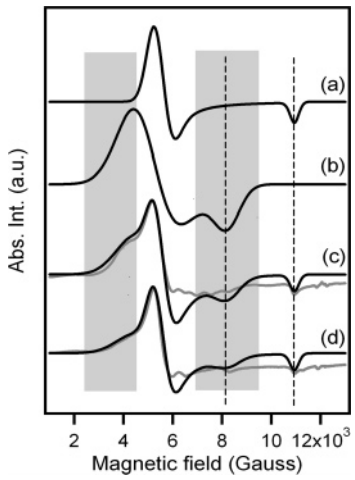

Figure 9. EPR spectrum simulations of (a) tetrahedrally and (b) octahedrally surrounded Co^{2+} ions in the ZnO structure, (c) weighted fit [61.5% (a) and 38.5% (b)], after normalization at their maximum intensity, for the experimental spectrum of an as-obtained powder (shown in gray), and (d) a weighted fit [76% (a) and 24% (b)] for the spectrum of an annealed powder (experimental spectrum shown in gray).

splitting *D*. For thin films, Jedrecy et al.[25] found the following spin Hamiltonian values : $g_\perp = 2.2669$, $g_\parallel = 2.2212$, and $D = 2.75\ cm^{-1}$.

In Figure 9a, we show that a simulation using the zero-field splitting of Jedrecy et al.[25] but slightly modified *g*-values ($g_\perp = 2.292$, $g_\parallel = 2.226$) only matches the features indicated with black arrows in Figure 6. Although the differences in *g*-values are non-negligible, they are considerably smaller than the line widths. Therefore, we consider it safe to attribute these EPR features to the same substitutional Co^{2+} ions that were observed by optical absorption and luminescence experiments.

4.2. Surface-Adsorbed Co^{2+}. As demonstrated by UV−vis spectroscopy and ICP−MS, amine treatment transfers 50−60% of the Co^{2+} ions present in a threefold-washed Co:ZnO suspension from the Co:ZnO nanocrystals to the supernatant. Since the band gap of the quantum dots is not reduced by amine treatment, etching of the particles cannot account for this Co^{2+} transfer. Therefore, we conclude that complexation by OA removes adsorbed Co^{2+} ions from the nanocrystal surface. This means that at least 50% of the Co^{2+} ions present in as-synthesized 2% Co:ZnO are adsorbed at the nanocrystal surface instead of being incorporated in the nanocrystal core, and that these Co^{2+} ions cannot be removed by a simple washing procedure. The conclusion that an important fraction of the Co^{2+} ions are only surface adsorbed is supported by the almost threefold increase of the substitutional Co^{2+} absorption after ZnO shell growth around as-synthesized Co:ZnO cores containing surface-adsorbed ions. Since this procedure leaves the overall Co^{2+} content unchanged, this observation can only be accounted for if surface-adsorbed Co^{2+} ions are substitutionally incorporated in the growing Co:ZnO nanocrystals. The incorporation of surface-adsorbed Co^{2+} ions in the nanocrystal core by ZnO shell growth is confirmed by the fact that amine treatment of core/shell particles does not induce any transfer of Co^{2+} ions to the supernatant.

4.3. Type III Co^{2+}. Since a simulation of the EPR spectra based on substitutional Co^{2+} cannot account for the features indicated in gray in Figure 9, an additional component must be present in the EPR spectrum. This additional component has an EPR intensity of the same order of magnitude as substitutional Co^{2+}. Comparison of spectra of many samples indicates that it is well-described by the anisotropic *g*-values $g_\parallel^{\text{eff}} \approx 3$ and $g_\perp^{\text{eff}} \approx 5$. Since we have no evidence for the presence of other EPR active species other then Co in such high concentrations, we attribute this signal to Co as well.

Contamination of the sample with possible byproducts of the Co:ZnO synthesis, like metallic Co, CoO, or Co_3O_4, cannot explain this feature. Given the synthesis conditions, the presence of metallic cobalt is very unlikely. Moreover, it should give an additional contribution to the XPS spectrum with a binding energy ~2 eV lower than that of Co^{2+}.[15] The cobalt oxides CoO and Co_3O_4 have markedly different EPR spectra: Co_3O_4 has only a broad signal at $g \approx 2$,[26] while CoO should yield an isotropic EPR signal at $g \approx 4.33$. Therefore, we identify this EPR feature with Co^{2+} ions that have a direct relation with the Co:ZnO nanocrystals. However, although removing an amount of surface-adsorbed Co^{2+} that corresponds to 50−60% of all Co^{2+} ions present, amine surface treatment does not change the EPR intensity ratio of the two components. This demonstrates that the presence of surface-adsorbed Co^{2+} ions does not account for the additional features in the EPR spectrum. We conclude that, besides substitutional and surface-adsorbed Co^{2+}, an additional type of Co^{2+} ion—type III Co^{2+}—is present in the core of Co doped ZnO nanocrystals.

On the basis of the EPR spectra, a further understanding of these type III Co^{2+} ions can be obtained. For Co^{2+} ions in an octahedral coordination, the $^4T_1$ triplet lies lowest. Spin-orbit coupling further splits this level, resulting in an effective spin doublet ($S = {}^1/_2$) ground state for which the spin Hamiltonian does not include a zero-field splitting term ($D = 0$). Theoretical analysis of the *g*-tensor shows that, in this case, its principal values satisfy the condition

$$\sum_i g_i \approx 13 \quad (i = x, y, z) \tag{2}$$

Centers of this type have, e.g., been found in ammonium Tutton salt[27] ($g_\perp = 3.06$, $g_\parallel = 6.45$) and in AgCl[28] ($g_\perp = 3.89$, $g_\parallel = 5.37$).

The principal *g*-values of the additional component in the Co:ZnO EPR spectrum satisfy the above relation for octahedral coordination. In Figure 9, an EPR spectrum simulation of this second component is shown and appropriate mixing of these two components leads to satisfactory agreement with the experimental spectra. These results suggest that the type III Co^{2+} ions inside the core of the

(25) Jedrecy, N.; von Bardeleben, H. J.; Zheng, Y.; Cantin, J. L. *Phys. Rev. B* **2004**, *69*, 041308.
(26) Oliva, C.; Cappelli, S.; Kryukov, A.; Chiarello, G. L.; Vishniakov, A. V.; Forni, L. *J. Mol. Catal. A: Chem.* **2006**, *255*, 36.
(27) Pilbrow, J. J. R. *Transition Ion Electron Paramagnetic Resonance*; Oxford Science Publications, Claredon Press: Oxford, U.K., 1990.
(28) Vanrobbroeck, L.; Goovaerts, E.; Schoemaker, D. *Phys. Status Solidi B* **1985**, *132*, 179.

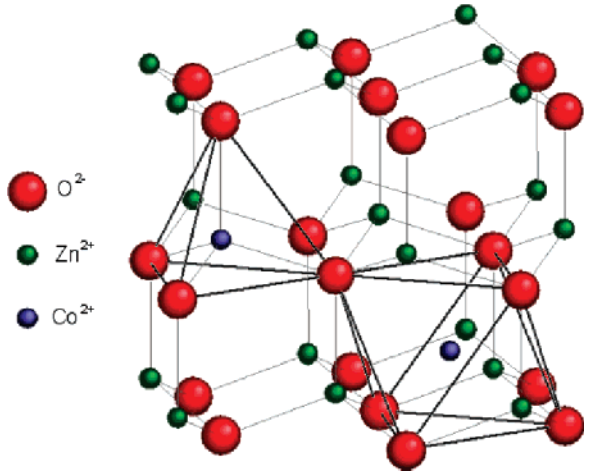

Figure 10. Drawing of an interstitial and a substitutional cobalt ion in an octahedral and tetrahedral hole in the ZnO wurtzite structure, respectively.

ZnO nanocrystals have an octahedral coordination. Taking a closer look at the ZnO wurzite crystal structure, one sees that it contains large octahedral holes enclosed by oxygen atoms (Figure 10). Since these holes can hold interstitial zinc ions, a widespread defect in ZnO,[29] it is not unlikely that the type III Co^{2+} ions apparent from EPR measurements correspond to octahedrally coordinated interstitial Co^{2+}. This type of Co^{2+} defect has already been reported by Fouchet et al. based on Rutherford backscattering results for Co:ZnO thin films deposited on Al_2O_3 substrates.[30]

4.4. Shell Growth. Absorption spectroscopy between 500 and 800 nm provides a means to track changes of the number of substitutional Co^{2+} ions. After growing a ZnO shell, it almost triples. Shell growth leads to a moderate change of the intensity ratio of substitutional and type III Co^{2+} in the EPR spectrum, but it is not a threefold increase. This demonstrates that both types of Co^{2+} ions are formed by incorporation of surface-adsorbed Co^{2+} ions in the nanocrystal during the growth of a ZnO shell around a Co doped ZnO core. Clearly, this observation supports the interpretation that type III Co^{2+} is not a surface-adsorbed Co^{2+} species.

According to Gamelin and co-workers,[5] surface-adsorbed Co^{2+} acts as a precursor state prior to incorporation of Co^{2+} ions in the ZnO crystal lattice. Our results confirm this idea but show that it holds for both substitutional and type III Co^{2+} ions. When resuming the interpretation of type III Co^{2+} ions as Co^{2+} interstitials, this is not unreasonable, since especially the oxygen terminated (001) plane offers adsorption sites that may lead to the incorporation of interstitial Co^{2+}.

4.5. Heating. We assessed the influence of heat treatment on the EPR spectra by measuring the absorbance of dropcast Co:ZnO quantum dot layers. As shown in Figure 11, the absorbance related to $d-d$ transitions in substitutional Co^{2+} strongly increases after annealing. This demonstrates that the changing EPR signal intensity ratio reflects an increase of substitutional Co^{2+}. Since XRD measurements after annealing (Figure 2a) demonstrate considerable particle growth

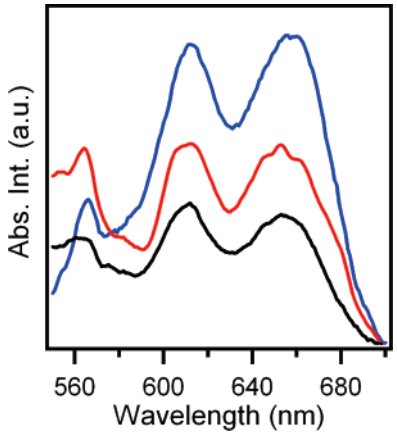

Figure 11. Absorbance spectra obtained on dropcast layers of 2% Co doped ZnO QDs: (—) as obtained, (blue line) after thermal treatment, and (red line) after amine and subsequent heat treatment.

during heat treatment, this can be explained in two ways. First, the increase of the tetrahedral vs octahedral EPR intensity could indicate that type III Co^{2+} ions diffuse to the surface of the nanocrystals to be incorporated substitutionally in the crystal lattice. Second, Co^{2+} ions that are adsorbed at the nanocrystal surface can become incorporated in the lattice by heating and crystal growth. This process changes the number of substitutional Co^{2+} ions but leaves the number of type III Co^{2+} ions unaltered. Performing a heat treatment on a dropcast layer of amine treated Co:ZnO particles, for which only a small fraction of the Co^{2+} ions originally adsorbed remains at the surface, results in an intermediate absorbance. This shows that adsorbed Co^{2+} ions are certainly incorporated substitutionally during particle growth, without ruling out the possibility of diffusion of type III Co^{2+} ions at elevated temperatures.

5. Conclusions

We have demonstrated the presence of three different types of Co^{2+} ions in 2% Co:ZnO colloidal quantum dots made from acetate precursor salts. First, Co^{2+} may substitute for Zn^{2+} on regular ZnO lattice positions. This leads to tetrahedrally coordinated Co^{2+} ions that dominate the absorbance and emission spectra and appear in the EPR spectrum with g-values close to those reported in literature. Second, a large fraction (50−60%) of the Co^{2+} ions are only adsorbed at the nanocrystal surface and can be detached by amine complexation. These Co^{2+} ions are not observed in the EPR spectra but contribute to the magnetic susceptibility of a nanocrystal powder. Finally, EPR measurements demonstrate the presence of a third type of Co^{2+}. This so-called type III Co^{2+} has an octahedral environment and is incorporated in the nanocrystal core. We therefore suggest that it corresponds to interstitial Co^{2+}. By growing a ZnO shell around the Co:ZnO cores, the surface-adsorbed Co^{2+} ions are incorporated in the nanocrystals, both as substitutional and as interstitial Co^{2+} ions.

These results demonstrate once more that dopant incorporation in colloidal nanocrystals by coprecipitation is far from straightforward. A large fraction of the dopant ions are only surface adsorbed, and those that are incorporated in the

(29) Zhang, S. B.; Wei, S. H.; Zunger, A. *Phys. Rev. B* **2001**, *6307*, 075205.
(30) Fouchet, A.; Prellier, W.; Padhan, P.; Simon, C.; Mercey, B.; Kulkarni, V. N.; Venkatesan, T. *J. Appl. Phys.* **2004**, *95*, 7187.

nanocrystal core may well appear as insterstitial defects rather then true substitutional dopants. Moreover, the work illustrates the importance of detailed studies on doping of quantum dots with impurity ions. In this work, only EPR spectroscopy revealed the existence of a third type of cobalt ions. Therefore, ensuring that dopants end up at the lattice site where one expects them to be remains a challenge one needs to address in order to understand the influence of dopants on the properties of colloidal quantum dots.

Acknowledgment. The authors thank D. Demuynck and Prof. F. Vanhaecke for performing ICP−MS measurements, Dr. S. Godey for performing XPS measurements, Prof. M. Van Bael for the SQUID measurements, and K. Lambert for the TEM measurements.

CM071623F